ORIGINAL PAPER

Enhancement of load bearing of post-grouted drilled shafts based on in situ tests

Zhitong Zhang[1,2] · Weiming Gong[1,2] · Guoliang Dai[1,2] · Jiang Xu[3]

Abstract

Field load tests were conducted for three large-diameter drilled shafts in the flood detention area of the grand bridge project of Beijing–Hangzhou Canal. Bi-directional testing of two grouted drilled shafts (TS1 and TS2) and one ungrouted drilled shaft (TS3) was used to study how post-grouting improved the bearing capacity of the drilled shafts. Based on the test results, the enhanced mechanism of the combined grouted drilled shafts was analyzed, and the analysis of load–displacement response was presented. It shows that grouting can significantly decrease the settlement of the drilled shafts and enhance resistance. By comparing the test results of the grouted and ungrouted shafts, it is found that the mechanical properties of the soil around the shaft can be improved effectively by post-grouting with the pressurized cement grout of the tip and side of the shaft. Furthermore, the effects of preloading on the load transfer characteristics of a shaft are also discussed. It can improve the asynchrony and incongruity between the side resistance and the tip resistance and promote the mobilization of tip resistance. The ratios of the tip resistance to the ultimate bearing capacity of test shafts TS1 and TS2 after post-grouting reached 37.11% and 41.72%, respectively, while the ratio of the ungrouted test shaft TS3 was 23.83%.

Keywords Drilled shaft · Bi-directional testing · Enhanced mechanism · Combined tip-and-side post-grouting · Preloading

Introduction

Drilled shafts are widely used for high-rise buildings and highway bridges because of their high bearing capacity and versatility. The borehole is often filled with slurry after drilling

✉ Weiming Gong
  Wmgong@seu.edu.cn

  Zhitong Zhang
  zhangzhitong2020@outlook.com

  Guoliang Dai
  daigl@seu.edu.cn

  Jiang Xu
  yzujxu@yzu.edu.cn

1   Key Laboratory of Concrete and Prestressed Concrete Structures of Ministry of Education, Southeast University, Nanjing 210096, China

2   School of Civil Engineering, Southeast University, Nanjing 210096, China

3   College of Civil Science and Engineering, Yangzhou University, Yangzhou 225000, China

to prevent the wall of the borehole from collapsing. However, in general, any mud around a pile decreases the pile shaft friction. In addition, the soil can relax beneath the shaft tip due to the drilling. This has a negative impact on the resistance, which is reduced even further if debris remains after a cleanout. There seems to be general agreement that the axial load on a drilled shaft is mainly supported by side shear and tip resistance in working conditions. Hence, the method of construction has a negative impact on the bearing capacity of drilled shafts (Mullins et al. 2000; Safaqah et al. 2007; Sliwinski and Philpot 1980; Bruce 1986; Duan and Kulhawy 2009; Zhang et al. 2009; Wan et al. 2017). Furthermore, even under ideal conditions for constructing a shaft, the ultimate side shear is mobilized in only a fraction of the displacement required to develop the ultimate end bearing. This leads to some of the tip resistance being wasted and a significant decrease of the bearing capacity of a drilled shaft (Mullins et al. 2000; Safaqah et al. 2007; Bruce 1986; Hirayama 1990).

Post-grouting is applied as follows. A grouting tube is connected to the side and tip of the pile. Grout is pressurized by a pump and injected into the tube. The grout infiltrates, compacts, and separates the mud around the shaft and the sediment

at the shaft tip. It compresses any soft debris or loose sand beneath the shaft tip, resulting in the earlier contact between the shaft tip and the founding soil. In this way, post-grouting enhances the strength of the soil at the shaft side and the shaft tip, which increases the bearing capacity of the pile foundation and reduces settlement. Post-grouting was first applied in engineering practice in 1958, and it has proven to be an effective way to enhance the axial resistance of the piles and reduce settlement (Safaqah et al. 2007; Bruce 1986; Wan et al. 2017, 2020; Bolognesi and Moretto 1973; Mullins et al. 2006; Dapp et al. 2006; Thiyyakkandi et al. 2013, 2014; Dai and Wan 2017).

Many researchers have studied post-grouting to improve the bearing capacity of drilled shafts. Thompson (1996) found that the key reinforcement mechanism of post-grouting is increasing the pile side friction along the shaft–soil interface through the migration of pressurized grout at the shaft tip. Zhang et al. (2009) carried out an in situ static load test to study the side friction resistance of super-long piles with different thicknesses of residues and different soil strengths at the pile end. Their results show that increasing the pile end strength can strengthen the pile side friction. Moreover, Dapp et al. (2006) found that preloading the tip is important for improving the bearing capacity of post-grouted drilled shafts. Additionally, Youn and Tonon (2010) analyzed the influence of post-grouting on the bearing behavior of bored piles using a field test and numerical simulations. Their results show that the negative friction caused by preloading the tip enhanced the side shear. Wan et al. (2017) clarified that the technology of post-grouting can be used on coral-reef limestone formations. Furthermore, Wan et al. (2020) investigated the behavior and performance of combined tip-and-side grouting of super-long large-diameter drilled shafts using four full-scale shaft load tests. This research indicated that the proportion of the load carried by the shaft tip can be significantly increased due to the combined grouting technique.

In conclusion, it is considered that four mechanisms are mainly responsible for enhancing the bearing capacity:

1. Compaction of soft deposits below the tip (Bolognesi and Moretto 1973; Thompson 1996; Gouvenot and Gabiax 1975; Stocker 1983; Sherwood and Mitchell 1989)
2. Due to the formation of a grout bulb at the tip, the tip area is increased (Zhang et al. 2009; Ruiz and Pando 2009).
3. Migration of the grout along the shaft side, which strengthens the soil (Duan and Kulhawy 2009; Zhang et al. 2009; Thompson 1996; Huang and Gong 2006; Dai et al. 2006; Lin et al. 2010)
4. Prestressing of the tip due to the reversal of shaft friction (Mullins et al. 2006; Thompson 1996; Youn and Tonon 2010; Fleming 1993; Pooranampillai et al. 2010; Fang et al. 2014).

However, research on the post-grouting of large-diameter drilled shaft mainly focuses on grouting only at the tip or only at the side. There has been less research on combined tip-and-side post-grouting. Thus, the mechanical properties, load transfer, and mobilization of shaft resistance of large-diameter drilled shafts after combined tip-and-side post-grouting need to be studied systematically through static field load tests. In particular, there have been few field tests of the long-term loading of large-diameter post-grouted drilled shafts.

In this research, full-scale load tests were conducted to investigate the field performance of two post-grouted drilled shafts. An ungrouted drilled shaft was used as the control. And, the bearing capacity of the three shafts was determined by bi-directional static tests. Based on the strain gauge data, the distribution of axial force and axial resistance are obtained. Thus, the relation between axial resistance and relative displacement is given, and the effect of post-grouting under an axial compression load is presented.

Full-scale field study

Overview of the site and test shafts

The shaft tests were conducted in the flood detention area of the grand bridge project of Beijing–Hangzhou Canal in Tai'an, China. The site has a width of 26.5 m and a total length of 21.586 km. There are three variable-cross-sectional prestressed concrete bridges with a main span of 110 m. The maximum span of the other approach bridges is 35 m. Post-grouting was proposed for the pile foundations.

Three test shafts were constructed at the site. Test shafts TS1 and TS2 have a length of 34 m and 36 m, respectively, and they are 1.6 m in diameter. Shaft TS3 is 1.8 m in diameter and 46 m in length. TS2 and TS3 rest on a layer of coarse sand, and TS1 rests on a layer of silty clay. Test shafts TS1 and TS2 were grouted using combined tip-and-side post-grouting, whereas TS3 was left ungrouted. The grouting system is similar to that described by Duan and Kulhawy (2009). There are three straight grouting pipes and two ring-shaped grouting pipes fixed at the bottom and side of the shaft, respectively. To investigate the load transfer of the shafts, the vibrating-wire strain gauges were installed at various locations along the axis. The elevations of the strain gauges along each shaft are presented in Fig. 1. Meanwhile, the mobilization curves of tip resistance were obtained with data from the strain gauges. Moreover, Fig. 1 shows that the ring-shaped grouting pipes were located at 10 m and 20 m above the shaft tips of TS1 and TS2, respectively.
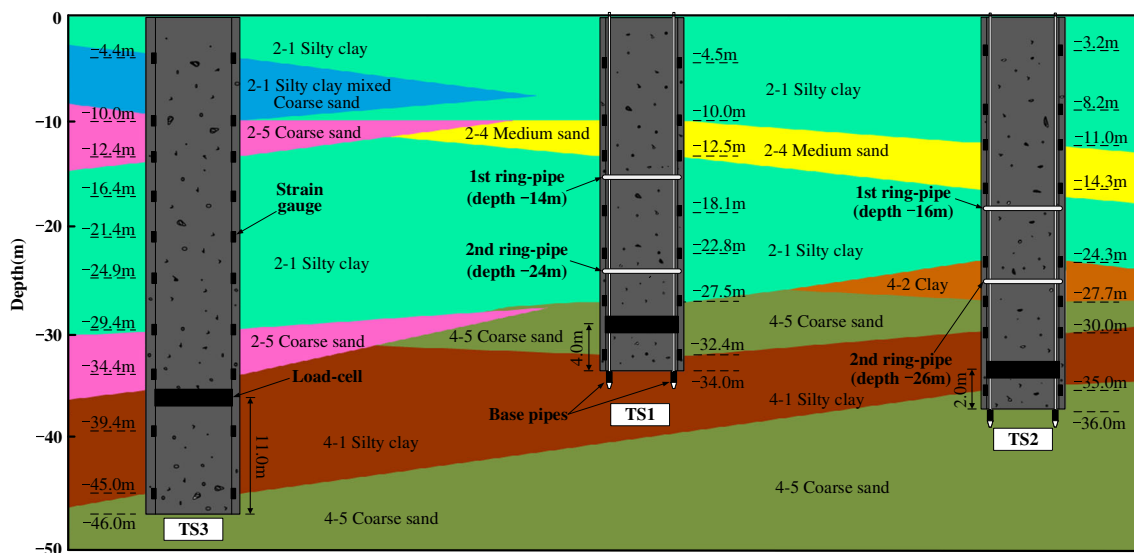
Fig. 1 Soil distribution and locations of strain gauges

It is also shown in Fig. 1 in which the soil profile consists of seven types of soils: (1) 2-1 silty clay, located at depths of 0~11 m and 12.4~29.4 m; (2) 2-1 silty clay–mixed coarse sand about 5.6 m thick between 4.4 and 10.0 m from the ground surface; (3) 2-4 medium sand, with the average thickness of approximately 2.9 m; (4) 2-5 coarse sand, located at depths of 10.0~12.4 m and 29.4~34.4 m; (5) 4-2 clay, located at depths of 24.3~27.7 m; (6) 4-5 coarse sand, located at depths of 27.5~32.4 m and 35.0~46.0 m; and (7) 4-1 silty clay, located at depths of 30~45.0 m, with the thickness of approximately 5.6 m. Details of the soil layers at the Tai'an site and the corresponding average physical characteristics and other details of the test shafts are listed in Tables 1 and 2, respectively. As shown in Table 1, ω is the moisture content, γ is the unit weight of soil, standard penetration test (SPT) N is the blow counts of the standard penetration tests. Then, φ and c are internal friction angle and cohesion of soil, respectively, which were obtained by triaxial compression test. The soil parameters (ω, γ, φ, c, etc.) were obtained from laboratory tests. Sample preparation, test equipment, and test methods were all in accordance with Chinese standard GB/T 50123-1999 (Ministry of Water Resources of the People's Republic of China 1999).

Field testing

As mentioned, this research used bi-directional static tests. During a test, the shaft was divided into two segments (upper and lower) by a load cell or O-cell (Fig. 2), which was welded to the shaft. The location details of the O-cells for the three shafts are illustrated in Fig. 1. The load cell was pressurized by a pump on the ground. As the pressure increased, the load cell expands so that its upper surface was displaced upward and its lower surface downward. This promotes the mobilization of the shaft side resistance and tip resistance.

The pressure in the load cell was measured with a pressure gauge. A total of six displacement transducers were installed on each test shaft, two of which were fixed at the top of the shaft, and the other four were installed at the upper and lower levels of the O-cell, as shown in Fig. 2a. The corresponding upward force versus displacement diagrams and downward force versus displacement diagrams can be plotted from the readings. And, Fig. 2b shows the placing of the steel rebar cage.

The bi-directional static tests were conducted for the three test shafts with a slowly changing load. The

Table 1 Physical properties of the soil at the Tai'an site

Layer	Stratum description	ω (%)	γ (kN/m³)	c (kPa)	φ (°)	SPT (N)	q_s (kPa)
2-1	Silty clay	25.7	19.0	41.1	11.7	8	35–50
2-4	Medium sand	23.7	19.2	7.5	16.1	16	40–50
2-5	Coarse sand	30	18.4	3.7	18.9	13	40–50
4-1	Silty clay	23.7	19.2	44.3	15.8	15	50–68
4-2	Clay	23.3	19.3	39.5	11.5	18	58–65
4-5	Coarse sand	22.0	18.5	4.3	25.9	19	60–70

Table 2 Parameters of the three test shafts

Shaft	Diameter (m)	Length (m)	Bearing soil layer	Concrete grade	Volume of concrete (m^3)	Position of O-cell above shaft tip (m)
TS1	1.6	34	4-1 silty clay	C30	70	4
TS2	1.6	36	4-5 coarse sand	C30	80	2
TS3	1.8	46	4-5 coarse sand	C30	120	11

loading and unloading followed the Chinese standard JT/T 738-2009 (The Traffic Professional Standards Compilation Group of the People's Republic of China 2009). The load was applied by the load cell and increased incrementally.

Test results

Tests of shafts TS1 and TS2 were conducted after post-grouting. The grouting parameters for both test shafts are given in Table 3. The test shaft TS1 was loaded in 17 increments (2 × 10.2 MN). At that point, there was the possibility of failure due to the large change in the downward displacement. In addition, since the expected loading value was achieved, the loading was terminated. Therefore, the 17th grade (10.2 MN) was taken as the limit load for both the upper and lower shaft segments of test shaft TS1. Then, we unloaded the test shaft TS1 in five increments and stopped the test. Similarly, for test shaft TS2, the limit loads for the upper and lower shaft segments were both 12 MN. And, the limit loads for the upper and lower shaft segments were 9.0 MN and 8.4 MN for test

shaft TS3, respectively. It should be noted that the capacity of the load cell used in this test is 2 × 12 MN, the test shaft TS2 reached the equipment loading limit, and the loading was stopped.

The results for the three test shafts are given in Table 4. The ultimate bearing capacities of the test shafts were obtained based on Eq. (1)

$$P_u = \frac{Q_{uu} - W}{\gamma_c} + Q_{lu} \tag{1}$$

where P_u is the limit bearing capacity of the test shaft (kN), Q_{uu} is the limit load of the upper shaft segment, Q_{lu} is the limit load of the lower shaft segment, W is the weight of the upper section of the test pile, and γ_c is a correction factor for the test shaft. For cohesive soil and silt, $\gamma_c = 0.8$, and for sandy soil, $\gamma_c = 0.7$. γ_c is a weighted average over the different soil layers.

From Table 4, it can be seen that the ultimate bearing capacities of TS1 and TS2 are higher than that of TS3, indicating that post-grouting can enhance the ultimate bearing capacity of a test shaft.
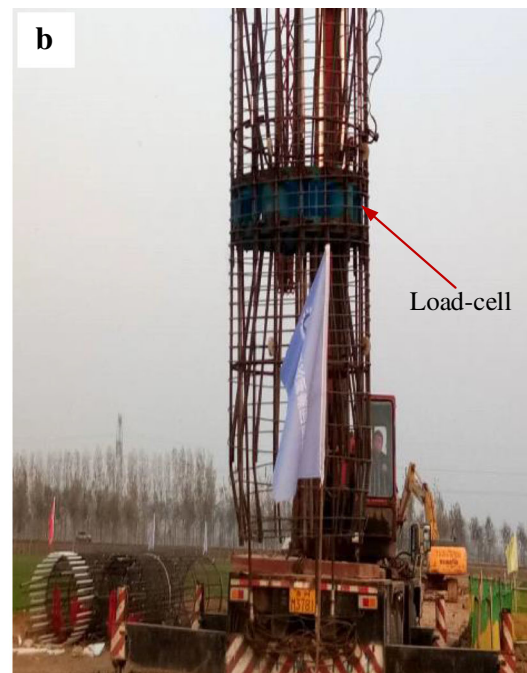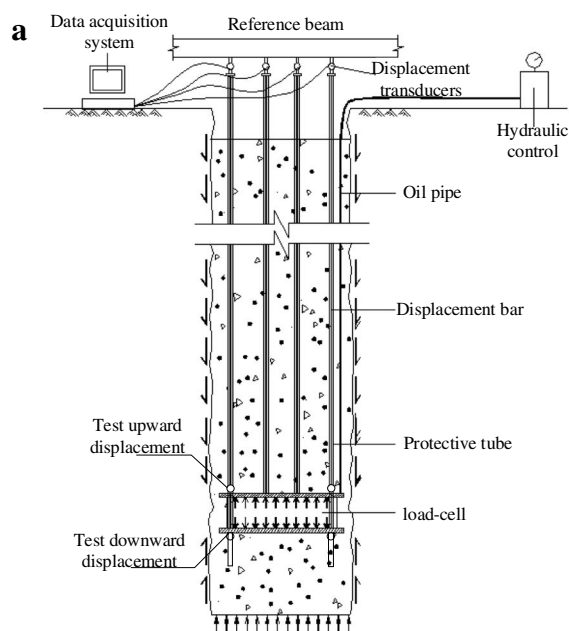

Fig. 2 Bi-directional static test of a shaft. **a** Sketch of a bi-directional static test. **b** Steel cage

Table 3 Grouting parameters of test shafts

Shaft	Quantity of cement (kg)	Grouting pressure (MPa)			Positions of side pipes above shaft tip (m)
		C1	C2	D1, D2, D3	First, second
TS1	7590	1.161	1.911	1.8–2.1	10, 20
TS2	7580	0.727	1.257	2.2–4.3	10, 20

Analysis of static load test results

Load versus displacement of the load cell

Figure 3 shows the relations between the load and normalized displacement for three test shafts. The normalized displacement is the ratio of the measured displacement to shaft diameter (D). The displacement measured here includes the upward and downward displacements of the load cell. Table 5 lists the measured displacements of the load cell for the three test shafts.

Figure 3 shows that the displacement of each shaft segment increases gradually with the increase of load. And, there is a clear inflection point in the load versus downward displacement curves of test shafts TS1 and TS3, which does not appear in the load versus displacement curves of TS2 or the load versus upward displacement curves of TS1, TS2, and TS3. This illustrates that the shaft resistances of the upper shaft segments were not fully mobilized and that the actual load of TS2 has not reached its ultimate bearing capacity.

Whether the bearing soil layer of the test shaft is cohesive or non-cohesive soil, Fig. 3 indicates that the displacements of the grouted shafts are lower than those of the ungrouted shaft under the same load. In other words, the settlement of the shaft can be effectively reduced by combined tip-and-side grouting to a shaft, for both cohesive and non-cohesive soils. Although the load versus displacement curves of TS1 (post-grouted shaft) and TS3 (ungrouted shaft) have similar trends, the lower shaft segment of TS1 has an obviously higher limit bearing capacity, which indicates that the bearing capacity of a shaft can be significantly enhanced by this grouting technique. Figure 3 also illustrates that the bearing capacities of the grouted shafts are larger than that of the ungrouted shaft at the same displacement and can be mobilized at a much smaller displacement. Thus, the load bearing of a shaft could be improved effectively by post-grouting.

Side resistance of the test shafts

In this paper, the axial force on the shaft was calculated using measurements made by a vibrating-wire strain gauge installed on the reinforcement cage in advance. These data were used to calculate and analyze the side resistance of the shaft and the shaft–soil relative displacement. The calculation steps and analysis process are as follows.

First, based on the vibration frequency measured by the vibrating-wire strain gauge under different loading levels, the strain ε_s at the gauge under a certain level of load can be obtained

$$\varepsilon_s = K\left(f^2 - f_0^2\right) \tag{2}$$

where K is a factor for the strain gauge, f is the frequency of the strain gauge under a load, and f_0 is the initial frequency.

It is assumed that the strain in the concrete in the test shaft is equal to that of the steel rebar under the same load. Thus, the axial force for shaft section i is

$$P_i = \varepsilon_s E_s A_s + \varepsilon_c E_c A_c \tag{3}$$

where ε_c is the strain in the concrete and $\varepsilon_c = \varepsilon_s$; E_s and E_c are the moduli of elasticity of the steel rebar and the concrete (kPa), respectively; and A_s and A_c are the cross-sectional areas of the steel rebar and concrete (m^2), respectively.

Then, the side resistance of the different soil layers can be determined from the axial force calculated with Eq. (3), combined with the parameters for the shaft section

$$q_{si} = \frac{\Delta P_i}{\Delta S_i} \tag{4}$$

where q_{si} is the side resistance at section i (kPa), ΔP_i is the difference in the axial force P between adjacent sections of the test shaft (kN), and ΔS_i is the side surface area between adjacent measurement sections of the test shaft (m^2). The resulting

Table 4 Calculated ultimate bearing capacities of the three test shafts

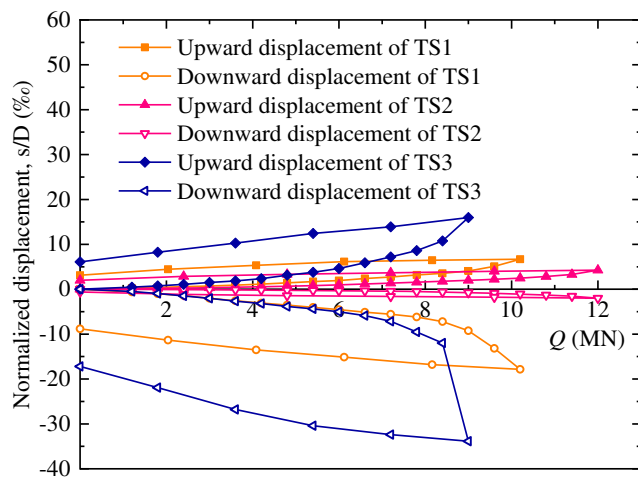| Shaft	Q_{uu} (kN)	Q_{lu} (kN)	Length of upper section shaft (m)	W (kN)	γ_c	P_u (kN)
TS1	10,200	10,200	30	875	0.78	22,156
TS2	12,000	12,000	34	991	0.78	26,114
TS3	9000	8400	35	1291	0.78	18,283

Fig. 3 Load versus displacement curves of the test shafts

axial resistance distributions of the three test shafts (TS1, TS2, and TS3) are shown in Fig. 4.

Figure 4 shows that the side resistance depends on the properties of the soil layer and on the depth. The side resistance also depends on the technology used to make the shaft and the relative displacement of the shaft and soil. Moreover, Fig. 4 clearly illustrates that the shaft side resistance is also affected by the position of the loading on the shaft, and in a bi-directional static test, the position of the load cell is a boundary. The side resistance for soil layers adjacent to the load cells was more fully developed, while soil layers further from the load cells had not reached the plastic state. Note that the side resistance of each soil layer after grouting is greater than that of the soil layers without grouting under various loads, which shows that the mechanical characteristics of the shaft side can be effectively improved and the side friction resistance of the shaft is significantly mobilized after combined tip-and-side post-grouting.

Relation between the shaft–soil relative displacement and the side resistance

It is important for shaft–soil relative displacement to the mobilization of the shaft side resistance. In this research, it was assumed that the relative displacement between the shaft and the soil at a particular depth was equal to the shaft displacement

Table 5 Loads and displacements of the three test shafts

Shaft	Load (kN)		Total displacement (mm)	
	Upward	Downward	Upward	Downward
TS1	10,200	10,200	10.71	28.53
TS2	12,000	12,000	6.82	3.18
TS3	9000	8400	28.73	60.97

at the same depth. And, the shaft–soil relative displacement can be obtained with

$$s_i = s_\mathrm{m} - \sum_{i=1}^{n} \frac{l_i(P_i + P_{i+1})}{2E_s A_s} \qquad (5)$$

where s_i is the shaft–soil relative displacement at soil layer i (mm); s_m is the measured displacement of the O-cell in the soil layer (mm); P_i and P_{i+1} are the axial forces on shaft sections i and $i+1$ (kN), respectively; and l_i is the length of the shaft section in soil layer i (m).

The side resistance of each test shaft as a function of the shaft–soil relative displacement is shown in Fig. 5. It can be observed that the mobilization of shaft side friction resistance depends on the shaft–soil relative displacement. With an increase of the relative displacement, the side friction gradually changes from being linear to nonlinear. For the upper shaft segments, the side resistance of the grouted shafts (TS1 and TS2) and ungrouted shaft (TS3) was basically in the elastic–plastic state. In contrast, the shaft resistance of the lower shaft segment was mobilized rapidly and then transitions into the plastic state. The side resistance for TS1 and TS2 is larger than that for TS3 under the same displacement. The displacement required for TS3 to change from the elastic–plastic state to the plastic state is much smaller than that for TS1 or TS2.

Figure 5d shows that for approximately the same depth and soil layer, the side resistance is related to the location of the ring-shaped grouting pipe. It is significantly higher for a soil layer adjacent to the grouting pipe. Additionally, the side resistance of soil layers away from the ring-shaped grouting pipe was also stronger, which indicates that the cement grout has migrated to the top of the shaft head. Thus, the amount of grout was a critical factor affecting the increase in the side resistance.

Equivalent conversion results

The results from the bi-directional static tests were converted into the equivalent shaft head loads and normalized settlements, according to the Chinese standard JT/T 738-2009. Curves for the equivalent shaft head load versus the normalized settlement are shown in Fig. 6.

As shown in Fig. 6, the equivalent ultimate loads applied at the test shaft heads of TS1, TS2, and TS3 are 22.156 MN, 26.114 MN, and 18.283 MN, respectively. Obviously, the ultimate bearing capacities of the post-grouted shafts TS1 and TS2 are higher than that of the ungrouted shaft TS3. It can also be observed that the equivalent normalized settlements at the shaft heads of test shafts TS1, TS2, and TS3 at the limit load are 2.2% D, 1.1% D, and 1.9% D, respectively. Note that the differences in the load versus settlement curves between the grouted shafts and the ungrouted shaft become more significant as the load increases. The settlement of the
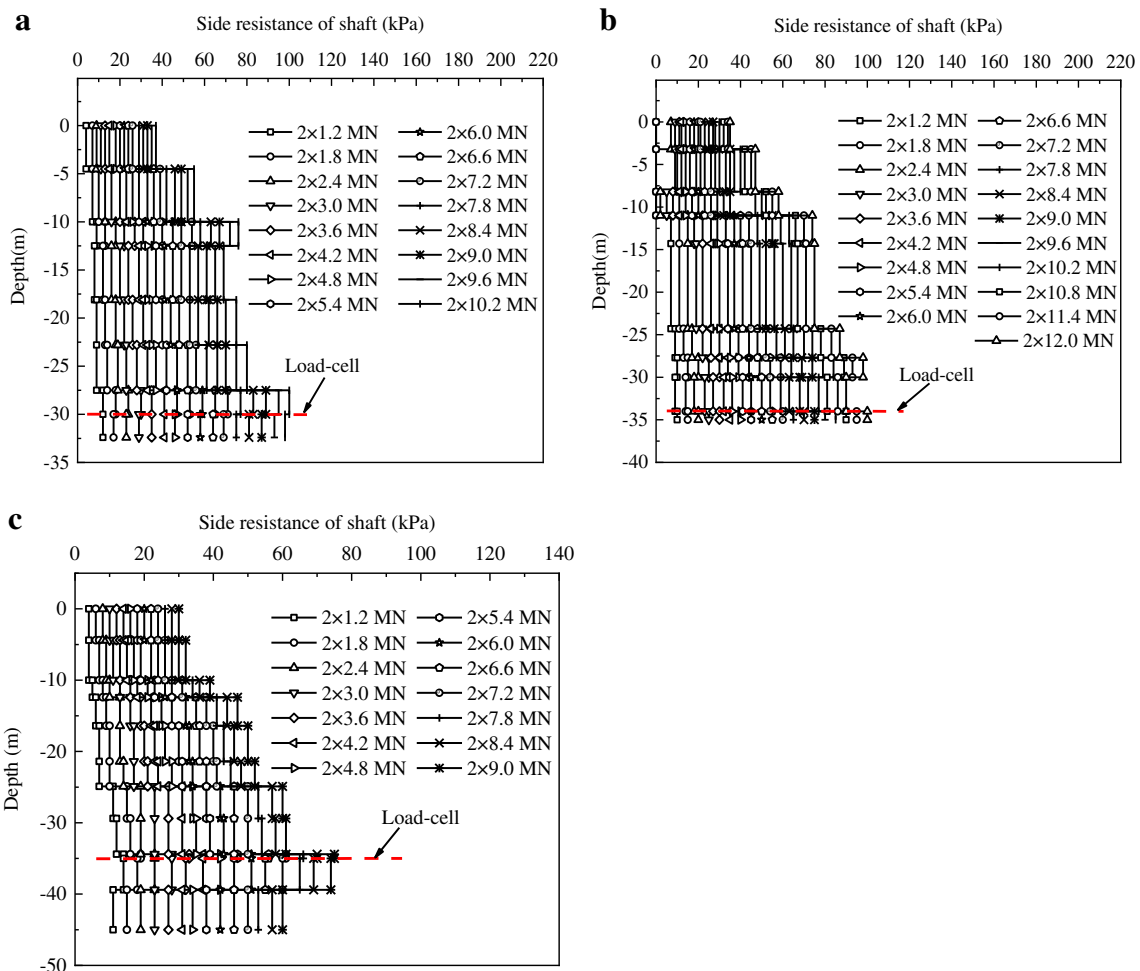
Fig. 4 Distributions of axial resistance for the three test shafts. **a** TS1. **b** TS2. **c** TS3

test shafts TS1 and TS2 was smaller than that of the test shaft TS3 under the same load, due to the injected cement grout. The results show that combined tip-and-side post-grouting can significantly reduce the settlement of the shaft head and greatly enhance the ultimate bearing capacity of the shaft.

Discussion

Compared with the ungrouted test shaft TS3, the post-grouted test shafts TS1 and TS2 were shorter and have a smaller diameter. However, the post-grouted shafts have a higher ultimate bearing capacity and a smaller displacement under the same load level. The test results demonstrate that both the side resistance and tip resistance of two large-diameter test shafts can be significantly improved by combined tip-and-side post-grouting. Reinforcing the sediment and soil under a shaft tip by post-grouting increases the resistance at the tip of the shaft. Moreover, increasing the hardness of the soil at the shaft tip not only can reduce the settlement of the shaft tip but also increase the total shaft side resistance, which improves the

ultimate bearing capacity of the drilled shafts. However, note that the shaft side resistance increases more significantly near the shaft tip. Many scholars have studied the influence of soil strength at the shaft tip on the side resistance of the shaft. Dong (2009) noted that as the strength and stiffness of the soil at the pile tip increased, the side resistance became significantly stronger. Moreover, Zhang and Zhang (2010) suggested that the main reason for the increase of the shaft side friction near the shaft tip was due to the enhancement of the soil strength at the tip of shaft by grouting.

The shaft–soil relative displacement required for each soil layer to reach the measured maximum of the side resistance is shown in Tables 6 and 7. Table 7 also shows the percentage increase of the ultimate side resistance of each soil layer due to post-grouting. As shown in Table 6, the measured side resistance of the ungrouted shaft TS3 is basically consistent with the geological exploration parameters. The error range is 0–20.0%, and the average relative error is 7.0%, which indicates that the test data are reliable. Table 7 shows that for the grouted shafts, the relative displacement required to develop the ultimate shaft resistance was significantly smaller than that
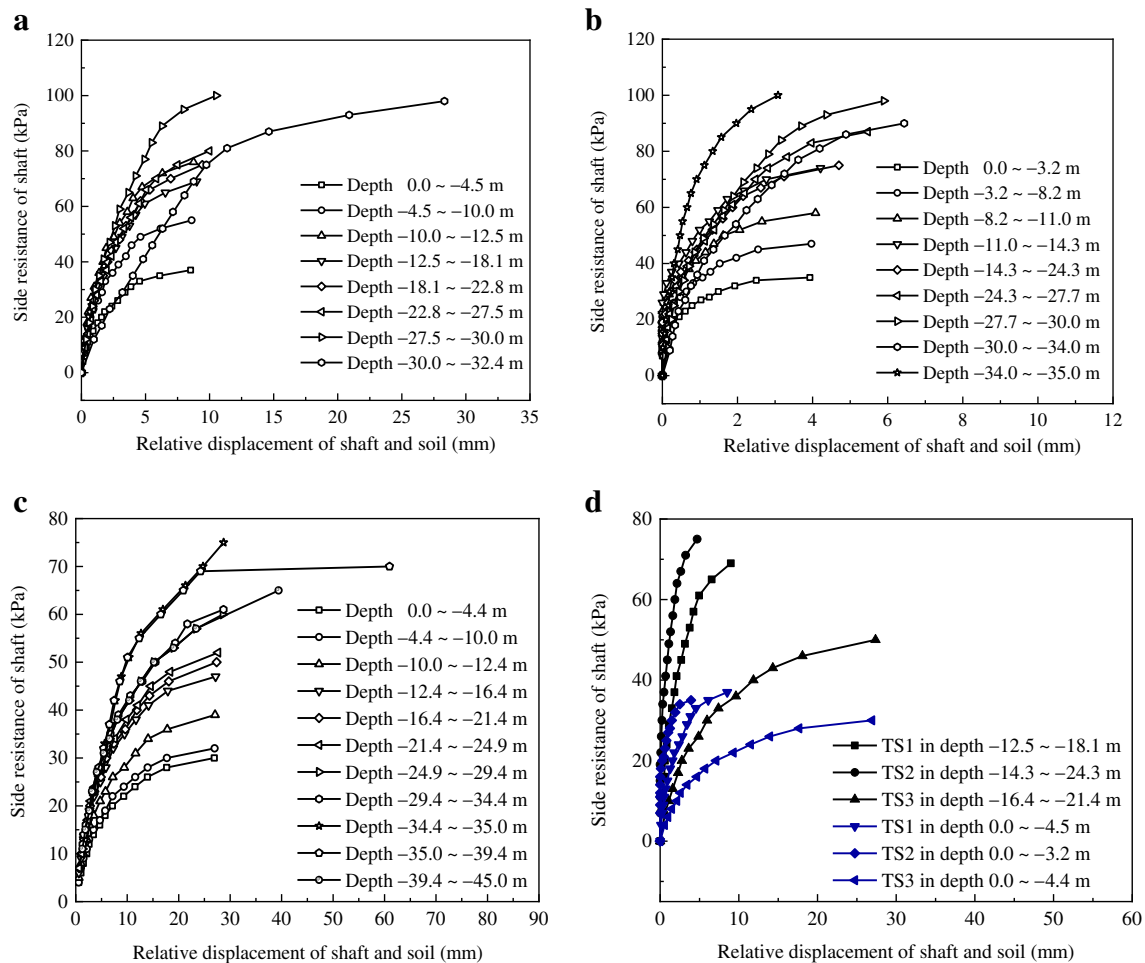
Fig. 5 Side resistance versus shaft–soil relative displacement. **a** TS1. **b** TS2. **c** TS3. **d** TS1, TS2, and TS3 for two depth ranges

for the ungrouted shaft. For example, for soil layer 2-1 at depths between −22.8 and −24.9 m, the measured maximum side resistances of the post-grouted pile TS1 and the ungrouted pile TS3 were 80 kPa and 52 kPa, respectively.

Fig. 6 Equivalent load versus normalized settlement for the test shafts

The corresponding displacements were 9.98 mm and 27.63 mm. This indicates that the displacement of the shaft can be effectively reduced and the soil around the shaft will be made stronger and stiffer due to post-grouting.

Additionally, note that the soil layer close to the shaft tip had a more obvious effect on the side resistance, indicating that the tip grouting improves the side resistance. For example, the side resistance for soil layer 4-5 near the tip of test shaft TS2 improved by 81.8%, whereas for the same soil layer further from the tip of test shaft TS2, the improvement was about 65.5%.

The primary objective of post-grouting is to improve the overall performance of a drilled shaft, by either increasing the ultimate axial resistance or improving the mobilization of shaft resistance, or both. It has been suggested that pre-mobilization of the load in the shaft will improve the mobilization of shaft resistance and thus improve the performance of the drilled shaft. This can be achieved by post-grouting. A theoretical basis for improving the mobilization of resistance of a drilled shaft using pre-mobilization was described by Fleming (1993). Subsequently, many scholars have researched the effect of preloading during post-grouting, as
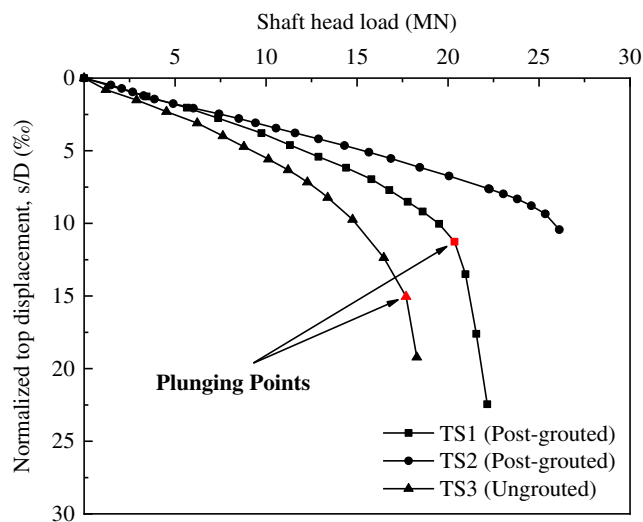
Table 6 Side resistance and the corresponding displacement of the ungrouted test shaft

Layer	Depth (m)	Characteristic value of side resistance (kPa)		Corresponding displacement (mm)	Relative error (%)
		Geological parameters	Measured maximum shaft resistance		
2-1	0 to −4.4	35	30	26.92	14.2
2-1	−4.4 to −10.0	40	32	26.98	20.0
2-5	−10.0 to −12.4	45	39	27.06	13.3
2-1	−12.4 to −16.4	50	47	27.16	6.0
2-1	−16.4 to −21.4	50	50	27.37	0
2-1	−21.4 to −24.9	55	52	27.63	5.5
2-1	−24.9 to −29.4	50	53	27.94	6.0
2-5	−29.4 to −34.4	60	60	28.39	0
4-1	−34.4 to −39.4	60	61	28.69	1.7
4-1	−39.4 to −45.0	60	66	60.97	10.0
4-5	−45.0 to −46.0	65	65	39.41	0

illustrated in Figs. 7 and 8 (Dai and Wan 2017; Fang et al. 2014; Chen et al. 2009).

Figure 7 shows the four stages of the resistance mobilization of a post-grouted drilled shaft. The first stage indicates a drilled shaft before grouting, and its performance corresponds to the curves labeled OC in Fig. 8a and b. In this case, the total load versus deflection response to top–down loading was established by summing the mobilized side and tip resistance for a given displacement. Figure 8 shows the limit values of shaft tip and side resistance before grouting (q_u and τ_f, respectively).

In the second stage, the bi-directional loading is induced during pressurized grouting at the shaft tip. This simultaneously mobilizes negative side resistance, which resists the upward loading, and positive tip resistance, which resists the downward loading. This case corresponds to the curves labeled OA in Fig. 8a and b. Figure 8 also shows that both positive (i.e., upward) and negative (i.e., downward) side

Table 7 Side resistance and the corresponding displacement of grouted test shafts

| Shaft	Layer	Depth (m)	Characteristic value of side resistance (kPa)		Corresponding displacement (mm)	Improvement of shaft resistance (%)
			Geological parameters	Measured maximum shaft resistance		
TS1	2-1	0 to −4.5	35	37	8.52	5.7
	2-1	−4.5 to −10.0	40	55	8.6	37.5
	2-4	−10.0 to −12.5	45	76	8.75	68.9
	2-1	−12.5 to −18.1	45	69	8.99	53.3
	2-1	−18.1 to −22.8	50	75	9.43	50.0
	2-1	−22.8 to −27.5	55	80	9.98	45.5
	4-5	−27.5 to −32.4	60	100	10.51	66.7
	4-1	−32.4 to −34.0	60	98	28.33	63.3
TS2	2-1	0 to −3.2	35	38	3.93	8.6
	2-1	−3.2 to −8.2	35	47	3.97	34.3
	2-1	−8.2 to −11.0	40	58	4.08	45.0
	2-4	−11.0 to −14.3	40	64	4.21	60.0
	2-1	−14.3 to −24.3	50	75	4.70	50.0
	4-2	−24.3 to −27.7	55	87	5.47	58.2
	4-5	−27.7 to −30.0	55	91	5.90	65.5
	4-1	−30.0 to −35.0	55	90	6.44	63.6
	4-5	−35.0 to −36.0	55	100	3.08	81.8
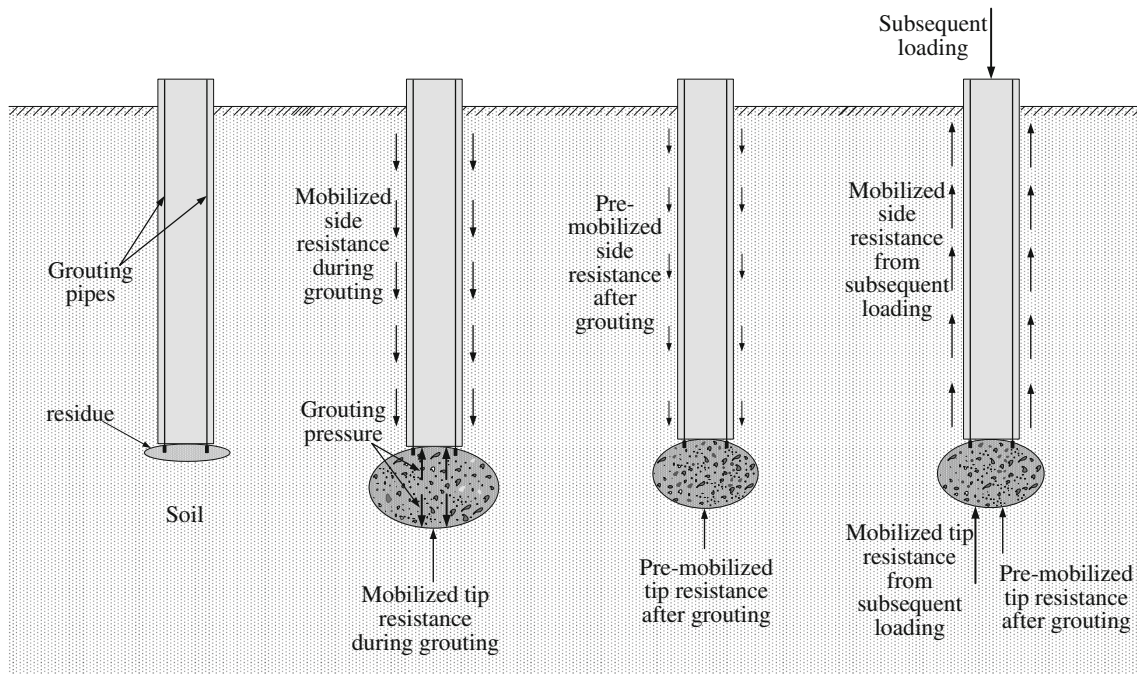
Fig. 7 Schematic illustrating the mobilization of resistance of a post-grouted drilled shaft

resistances can be mobilized, depending on the direction of loading; tip resistance is mobilized only if the loading is in the downward direction.

Following post-grouting, some relaxation of the resistance mobilized during grouting may occur, as indicated in the third stage. In this case, the mobilized side resistance and tip resistance will be reduced along the unloading curve AB, as illustrated in Fig. 8a and b, respectively. The point B on both curves reflects the net mobilized resistance that develops due to post-grouting. These points are the starting point for the subsequent loading of the shaft.

At the final stage, the shaft head is loaded with the subsequent structural load. This stage corresponds to the curves BD

and BF in Fig. 8a and b, respectively. As the subsequent load increases, the soil at the shaft tip is reloaded, and the side resistance is generally mobilized from negative to positive. It can also be observed from Fig. 8 that the side friction resistance and tip resistance of the shaft are increased by Δq_b and $\Delta \tau_2$, respectively, due to the preloading during post-grouting. The grouted shaft undergoes less tip displacement compared with the ungrouted shaft for the same applied load. Also note that the subsequent bi-directional loading will simply continue loading in the same direction as the loading during post-grouting. In addition, the surrounding soil will be split or infiltrated by the cement grout and mixed with it, all of which strengthen its resistance, making it harder and stronger. Thus,
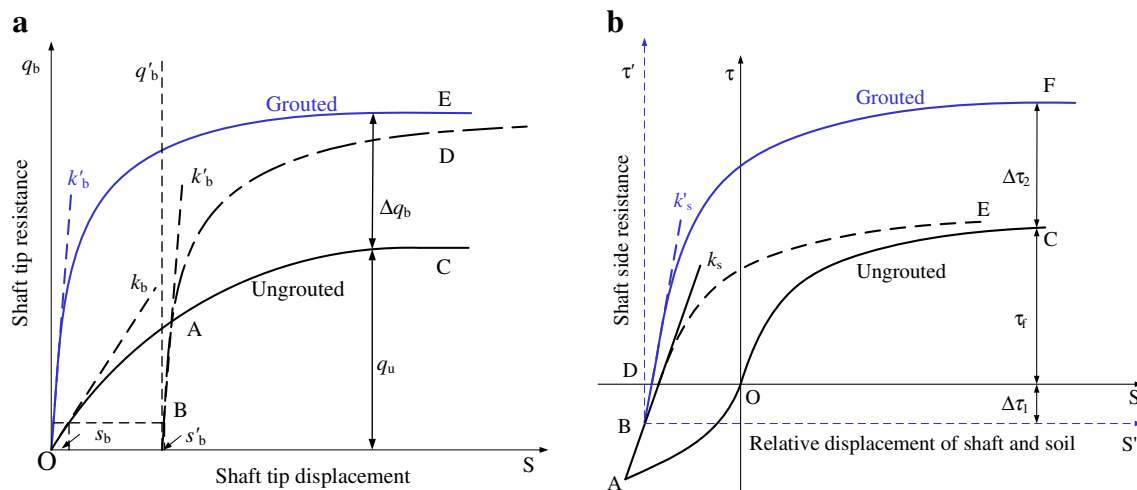

Fig. 8 Schematic illustrating the effect of preloading during post-grouting (Fang et al. 2014). **a** Tip resistance improvement. **b** Side resistance improvement

both of the above two mechanisms contribute to improving the side and tip stiffnesses. It is shown in Fig. 8 that the stiffness of the soil at the shaft side and tip is increased from k_s and k_b to k_s' and k_b' respectively.

In this research, the side resistance was subtracted from the tip resistance measured for the lower shaft segment under the O-cell loading. Because the lower shaft segment is relatively short, the actual mobilization of the shaft tip resistance of the lower shaft segment due to loading by the O-cell is reflected more directly. This aids the analysis of the effect and influence on the increase of the shaft tip resistance by post-grouting.

Figure 9 shows that the curves for the relation between tip resistance and normalized displacement of shaft tip for the three test shafts have a similar trend whether the shaft is grouted or not. However, the curves for the ungrouted shaft (TS3) are steep, unlike those for the post-grouted shafts (TS1 and TS2), which shows that the tip resistance of the post-grouted shafts was improved. Figure 9 also shows that for the same bearing load of the shaft tip, the tip displacement of the post-grouted shafts (TS1 and TS2) was significantly smaller than that of the ungrouted shaft (TS3), which indicates that for a post-grouted shaft, the tip bearing capacity can be mobilized with a smaller displacement. Moreover, the initial stiffnesses of the soil at the tips of TS1, TS2, and TS3 are shown in Fig. 9, i.e., k_1, k_2, and k_3, respectively. k_1 and k_2 are greater than k_3, which may be the result of penetration, compaction, and splitting of the soil by the pressurized grout and due to the sediment caused by the shaft-forming process at the bottom of the shaft. This further indicates that the effect of the combined grouting at the side and tip of the shaft is significant, as it improves the strength and stiffness of the soil at the shaft tip and has a significant impact on the bearing and load transfer characteristics of the shaft tip.
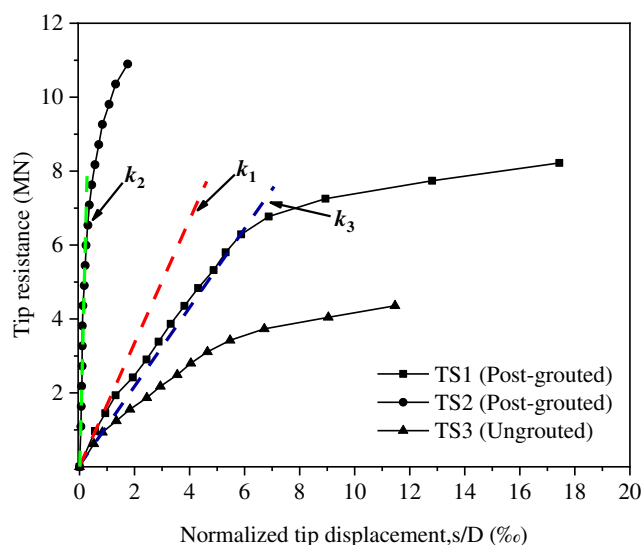
To study further the preloading due to post-grouting, this paper presents the ratio of mobilized shaft tip resistance to shaft head load under different loads. The load sharing ratios for the side resistance and the tip resistance of test shafts are illustrated in Fig. 10. The ratios of the tip resistance and side resistance to the shaft bearing capacity under the ultimate bearing capacity are given in Table 8.

Since bi-directional static tests were used, the load cell exerted a vertical thrust on the upper shaft segment, which moved upward relative to the soil layer. The soil layers around the shaft were loose and disturbed, which led to a significant reduction in the side resistance of the shaft–soil interface. Therefore, as shown in Fig. 10, the ratio of shaft tip resistance to the total bearing capacity of the shaft gradually decreased, while the ratio of shaft side resistance gradually increased, which is different from the result for a top–down load test.

Figure 10 illustrates that the ratio of tip resistance to shaft bearing capacity of the grouted shafts under different loads is higher than that of the ungrouted shaft. As shown in Table 8, under the condition of ultimate bearing capacity, the ratios of the tip resistance to the head load of test shafts TS1 and TS2 are 37.11% and 41.72%, respectively, whereas the ratio for test shaft TS3 is only 23.83%. This shows that the shaft head load is more rapidly supported after grouting by the tip resistance during the initial load due to the preloading by the tip grouting. Post-grouting can effectively reduce the displacement required for the mobilization of tip resistance, improve the asynchrony and incongruity of the mobilized side and tip resistance, and promote the mobilization of tip resistance, and thus, it can reduce the settlement of a drilled shaft when the subsequent loading is applied.

In addition, based on the data in Tables 6, 7, and 8, the limit bearing capacity of test shafts TS1, TS2, and TS3 can be obtained
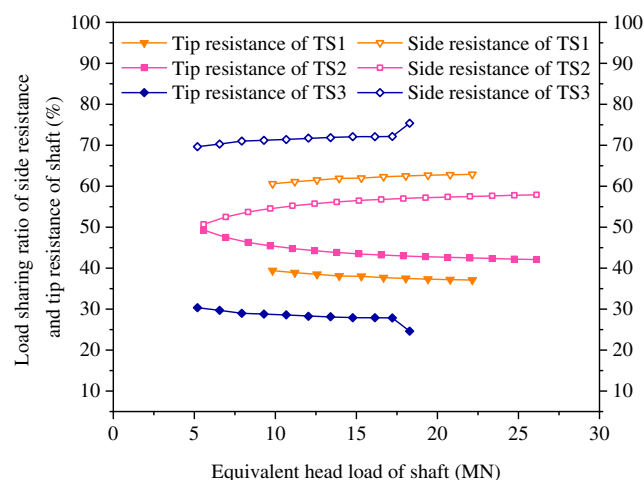
Fig. 9 Tip resistance versus normalized displacement of shaft tip for the three test shafts

Fig. 10 Load sharing ratio of side resistance and tip resistance of the three test shafts

Table 8   Proportion of bearing capacity of test shafts

Shaft	P_u (kN)	P_s (kN)	P_t (kN)	P_s/P_u (%)	P_t/P_u (%)
TS1	22,156	13,934	8222	62.89	37.11
TS2	26,114	15,218	10,896	58.28	41.72
TS3	18,283	13,927	4356	76.17	23.83

$$P_Q = u \cdot \sum_i^n l_i \cdot f_i + P_t \qquad (6)$$

where P_Q is the calculation value of limit bearing capacity of the test shaft (kN), u is perimeter of test shafts (m), l_i is the length of the shaft section in soil layer i (m), f_i is the characteristic value of side resistance of soil layer i (kPa), and P_t is the tip resistance of test shafts (kN).

Then, the calculation results are compared with the limit bearing capacity of the bi-directional static tests. Comparison results are given in Table 9. Table 9 shows that the relative error between the calculated limit bearing capacity and the value obtained by bi-directional static test is less than 9%, which proves the reliability of the test results of the bi-directional static test.

Conclusions

As part of the project for the flood detention area of Ningliang Road and the grand bridge of Beijing–Hangzhou Canal, this paper reports on three full-scale load tests conducted on the same site in Tai'an, China, and the field performance of grouted and ungrouted large-diameter drilled shafts is investigated. From the results and analysis, the following conclusions can be drawn:

(1) Combined tip-and-side post-grouting can significantly reduce the settlement of the shaft head for the same applied load and greatly enhance the ultimate bearing capacity of the shaft. The equivalent ultimate loads applied at the shaft heads of test shafts TS1, TS2, and TS3 were 22.156 MN, 26.114 MN, and 18.283 MN, respectively. The corresponding equivalent normalized settlements at

Table 9   Comparison of calculation value and the value of bi-directional static test

Shaft	P_u (kN)	$u \cdot \sum_i^n l_i \cdot f_i$ (kN)	P_t (kN)	P_Q (kN)	Relative error (%)
TS1	22,156	12,168	8222	20,390	7.97
TS2	26,114	12,910	10,896	23,806	8.84
TS3	18,283	13,025	4356	17,381	4.93

the shaft heads were 2.2% D, 1.1% D, and 1.9% D, respectively.

(2) The mechanical characteristics of the shaft side can be effectively improved, and the side friction resistance of the shaft is significantly mobilized after combined tip-and-side post-grouting.

(3) The distribution of the side resistance of a grouted shaft depends not only on the properties of the soil layer around the shaft but also on the loading position of the shaft and the amount of grout.

(4) The relative displacement required to mobilize the ultimate shaft resistance of the grouted shafts was significantly smaller than that for the ungrouted shaft. This is because post-grouting makes the soil surrounding the shaft stronger and stiffer.

(5) Tip grouting improves the side resistance. Additionally, the side resistance of a soil layer that was close to the tip of the shaft was more obviously enhanced due to the improvement of soil strength at the tip of the shaft because of the grouting.

(6) Preloading due to post-grouting can have a significant impact on the load transfer characteristics of the shaft. Post-grouting can improve the mobilization of shaft resistance. That is, it can improve the asynchrony and incongruity between the side resistance and the tip resistance and promote the mobilization of tip resistance.

Nomenclature A_c, cross-sectional area of the concrete (m^2); A_s, cross-sectional area of the steel rebar (m^2); c, cohesion of soil, from consolidated undrained triaxial tests (kPa); D, shaft diameter (m); E_c, modulus of elasticity of the concrete (kPa); E_s, modulus of elasticity of the steel rebar (kPa); f, frequency (Hz); f_i, characteristic value of side resistance of soil layer i (kPa); f_0, initial frequency (Hz); i, index of shaft section; k_b, initial stiffness of the soil at the shaft tip; k_b', stiffness of the soil at the shaft tip after post-grouting; k_i, initial stiffness of the soil at the shaft tip for shaft i; k_s, initial stiffness of the soil at the shaft side; k_s', stiffness of the soil at the shaft side after post-grouting; K, factor for the vibrating-wire strain gauge; l_i, length of the shaft section in soil layer i (m); N, standard penetration test (SPT); P_i, axial force on shaft section i (kN); P_Q, calculation value of limit bearing capacity of the test shaft (kN); P_s, side resistance (kN); P_t, tip resistance (kN); P_u, ultimate bearing capacity of the test shaft (kN); q_s, characteristic value of side resistance (kPa); q_{si}, side resistance at section i (kPa); q_u, limit values of shaft tip resistance before grouting (kPa); Q_{lu}, limit load of the lower shaft segment (kN); Q_{uu}, limit load of the upper shaft segment (kN); s_i, relative shaft–soil displacement at soil layer i (mm); s_m, measured upward or downward displacement of the O-cell in the soil layer (mm); u, perimeter of test shafts (m); W, weight of the upper section of the test pile (kN); γ, unit weight (kN/m^3); γ_c, soil correction factor for the test shaft; ΔP_i, difference in the axial force P between

adjacent sections of the test shaft (kN); ΔS_i, side surface area between adjacent measurement sections of the test shaft (m^2); ε_c, strain in the concrete; ε_s, strain at the gauge; τ_f, limit values of shaft side resistance before grouting (kPa); φ, internal friction angle (°); ω, natural water content (%)

References

Bolognesi AJL, Moretto O (1973) Stage grouting preloading of large piles on sand. Proceedings of the 8th International Conference on Soil Mechanics and Foundation Engineering, Moscow. https://doi.org/10.1016/0148-9062(75)92342-6

Bruce DA (1986) Enhancing the performance of large diameter piles by grouting. Ground Eng 19(4):9–15. https://doi.org/10.1016/0148-9062(86)92518-0

Chen RP, Zhou WH, Chen YM (2009) Influences of soil consolidation and pile load on the development of negative skin friction of a pile. Comput Geotech 36(8):1265–1271. https://doi.org/10.1016/j.compgeo.2009.05.011

Dai GL, Wan ZH (2017) Enhanced mechanism and load-settlement relationship of post-grouting piles. Chin J Geo Eng 39(12):93–102. https://doi.org/10.11779/CJGE201712012

Dai GL, Gong WM, Xue GY, Tong XD (2006) Effect examination for a base post-grouted overlength drilling pile. Rock Soil Mech 27(5): 849–852. https://doi.org/10.16285/j.rsm.2006.05.035

Dapp SD, Muchard M, Brown DA (2006) Exeriences with base grouted drilled shafts in the Southeastern United States. Proceedings of the 10th international conference on piling and deep foundations, Amsterdam, Netherlands, pp 1385–1394

Dong JR (2009) Enhanced and weakened effect of skin friction of cast-in-situ piles. Chin J Geo Eng 31(5):658–662. https://doi.org/10.3321/j.issn:1000-4548.2009.05.002

Duan X, Kulhawy FH (2009) Tip post-grouting of slurry-drilled shafts in soil: Chinese experiences. In: Contemporary topics in deep foundations. Orlando. https://doi.org/10.1061/41021(335)6

Fang K, Zhang ZM, Zhang QQ, Liu XW (2014) Prestressing effect evaluation for a grouted shaft: a case study. Proc ICE Geotech Eng 167(3):253–261. https://doi.org/10.1680/geng.11.00090

Fleming WGK (1993) The improvement of pile performance by base grouting. J Civ Eng 97(2):88–93. https://doi.org/10.1680/icien.1993.23262

Gouvenot D, Gabiax FD (1975) A new foundation technique using piles sealed by cement grout under high pressure. Proceedings of the 7th annual offshore technical conference. https://doi.org/10.4043/2310-MS

Hirayama H (1990) Load-settlement analysis for bored piles using hyperbolic transfer functions. Soils Found 30(1):55–64. https://doi.org/10.3208/sandf1972.30.55

Huang SG, Gong WM (2006) Study on bearing behavior of super long–large diameter piles after grouting. Chin J Geo Eng 28(1):113–117. https://doi.org/10.3321/j.issn:1000-4548.2009.05.002

Lin SS, Liao JC, Wang KJ (2010) Axial capacity of drilled shafts in clay over gravel formation. Proceedings of the 2010 geo-Shanghai international conference: Deep foundation and geotechnical in situ testing. https://doi.org/10.1061/41106(379)26

Ministry of Water Resources of the People's Republic of China (1999) GB/T 50123-1999 standard for soil test method. China Planning Press, Beijing (in Chinese)

Mullins G, Dapp S, Lai P (2000) Pressure-grouting drilled shaft tips in sand. Geotechnical Special Publication 100:1–17. https://doi.org/10.1061/40511(288)1

Mullins G, Winters D, Dapp S (2006) Predicting end bearing capacity of post-grouted drilled shaft in cohesionless soils. J Geotech Geoenviron Eng 132(4):478–487. https://doi.org/10.1061/(ASCE)1090-0241(2006)132:4(478)

Pooranampillai S, Elfass S, Vanderpool W. (2010) The effects of compaction post grouting of model shaft tips in fine sand at differing relative densities: experimental results. Art of Foundation Engineering Practice Congress. https://doi.org/10.1061/41093(372)24

Ruiz ME, Pando MA (2009) Load transfer mechanisms of tip post-grouted drilled shafts in sand. International foundation congress & equipment expo: contemporary topics in deep foundation. https://doi.org/10.1061/41021(335)3

Safaqah O, Bittner R, Zhang X (2007) Post-grouting of drilled shaft tips on the Sutong Bridge: a case history. Proceedings of the geo-Denver 2007 congress: Contemporary issues in deep foundations, CO, USA. https://doi.org/10.1061/40902(221)33

Sherwood DE, Mitchell JM (1989) Based grouted piles in Thanet Sands, London. Proceedings of the 3rd international conference on piling and deep foundations, London, 1:463–472

Sliwinski ZJ, Philpot TA (1980) Conditions for effective end bearing of bored, cast in situ piles. Proceedings of ICE conference on recent developments in the design and construction of pile, London, 73–80

Stocker MF (1983) Influence of post-grouting on the load-bearing capacity of bored piles. Proceedings of the 8th European conference on soil mechanics and foundation engineering, Helsinki. https://doi.org/10.1016/0148-9062(85)93190-0

The Traffic Professional Standards Compilation Group of People's Republic of China (2009) JT/T 738-2009 static loading test of foundation pile-self-balanced method. China Communications Press, Beijing (in Chinese)

Thiyyakkandi S, McVay M, Bloomquist D (2013) Measured and predicted response of a new jetted and grouted precast pile with membranes in cohesionless soils. J Geotech Geoenviron Eng 139(8):1334–1345. https://doi.org/10.1061/(ASCE)GT.1943-5606.0000860

Thiyyakkandi S, McVay M, Bloomquist D (2014) Experimental study, numerical modeling of and axial prediction approach to base grouted drilled shafts in cohesionless soils. Acta Geotech 9(3): 439–454. https://doi.org/10.1007/s11440-013-0246-3

Thompson PA (1996) Base and shaft grouted piles. Proc ICE Geotech Eng 119:186–192. https://doi.org/10.1680/igeng.1996.28511

Wan ZH, Dai GL, Gong WM (2017) Full-scale load testing of two large-diameter drilled shafts in coral-reef limestone formations. Bull Eng Geol Environ 10:1–17. https://doi.org/10.1007/s10064-017-1206-1

Wan ZH, Dai GL, Gong WM (2020) Field and theoretical analysis of response of axially loaded grouted drilled shafts in extra-thick fine sand. Can Geotech J 57(3):391–407. https://doi.org/10.1139/cgj-2018-0382

Youn H, Tonon F (2010) Numerical analysis on post-grouted drilled shafts: a case study at the Brazo River Bridge, TX. Comput Geotech 37(4):456–465. https://doi.org/10.1016/j.compgeo.2010.01.005

Zhang ZM, Zhang QQ (2010) Influences of soil strength at pile end on friction of lateral surface of piles. Chin J Geo Eng S2:59–63

Zhang ZM, Yu J, Zhang GX (2009) Test study on the characteristics of mudcakes and in situ soils around bored piles. Can Geotech J 46(3): 241–255. https://doi.org/10.1139/T08-119